Bioorganic Chemistry 153 (2024) 107932

Contents lists available at ScienceDirect

Bioorganic Chemistry

journal homepage: www.elsevier.com/locate/bioorg

Review Article

Unveiling cofactor inhibition mechanisms in horse liver alcohol dehydrogenase: An allosteric driven regulation

Alice Vetrano [a], Matteo Capone [a,b,*], Matteo Farina [c], Francesco Gabriele [a], Nicoletta Spreti [a,*], Isabella Daidone [a]

[a] Department of Physical and Chemical Sciences, University of L'Aquila, via Vetoio (Coppito 1), L'Aquila 67100, Italy
[b] Present address: CNR Institute of Nanoscience, S3 Center, Via Campi 213/A, Modena 41125, Italy
[c] Department of Chemistry, Sapienza University of Rome, Piazzale Aldo Moro 5, Rome 00185, Italy

ARTICLE INFO

Keywords:
Kinetics
Molecular dynamics
Allostery
NADH
Alcohol Dehydrogenase

ABSTRACT

Horse Liver Alcohol Dehydrogenase (HLADH) is an extensively studied enzyme isolated from equine liver tissue, and holds a central role in numerous enzymatic processes, underscoring the need for thorough investigation. This study delves into the kinetic behavior and structural dynamics of HLADH, shedding light on complex mechanisms governing its catalytic activity and interactions with the cofactor. Notably, deviations from traditional Michaelis–Menten kinetics are observed, manifesting as a slowdown in catalytic rate under high NADH concentrations. Utilizing molecular dynamics simulations, an allosteric site is identified, clarifying how excessive cofactor levels impact protein dynamics and catalytic properties. Structural alterations induced by inhibitory NADH concentrations are revealed, indicating reduced protein flexibility and modifications in catalytic cavity size, thereby elucidating the inhibitory mechanism at high cofactor concentrations. This comprehensive investigation unveils intricate facets of HLADH's catalytic mechanisms, providing a platform for further exploration in enzymology and biocatalysis.

1. Introduction

Alcohol dehydrogenases (ADHs) are a wide group of enzymes that have a crucial role in the metabolism of alcohols in many organisms. These enzymes are primarily responsible for the oxidation of alcohols to their corresponding aldehydes or ketones, as well as the detoxification of xenobiotics, and have several applications in enzymology and biochemistry [1–5]. In the last years, the application of ADHs to organic synthesis attracted substantial interest due to the high enantioselectivity, large variety of accepted substrates and mild reaction conditions [6,7]. Horse liver alcohol dehydrogenase (HLADH), in particular, has been used as a paradigmatic system for gaining insights into the structure and function of alcohol dehydrogenases as a whole [8]. Numerous investigations have delved into its catalytic mechanism, substrate specificity, and kinetic properties [9,4,3]. Furthermore, the elucidation of the three-dimensional structure of HLADH, achieved through X-ray crystallography, has provided valuable information on its active site and catalytic mechanism.

HLADH, classified as a metalloenzyme, is structured as a homodimer, where each monomer consists of 374 amino acid residues divided into two chains, denoted as A and B, contributing to a substantial molecular weight of 163.32 kDa. Within the active site, there are two zinc atoms, each of which plays distinct roles. One of these zinc atoms performs a catalytic function, and it is coordinated with Cys46, Cys174, His67, and water in the apoenzyme state. In the holoenzyme state, it binds to the substrate. The other zinc atom, known as structural zinc, is bonded to four cysteine residues [2]. Notably, the electron densities surrounding both the catalytic and structural zinc ions adopt a nearly spherical shape, with the catalytic zinc exhibiting a tetrahedral coordination arrangement. The zinc structural site of ADH has been assigned a role in the maintenance of a proper tertiary/quaternary structure. Related enzymes not containing this zinc ion, like sorbitol dehydrogenase, display a different quaternary structure [10,11], and recombinant variants of ADH, where one Cys ligand at the time has been changed to Ala, are structurally labile [12]. Approximately sixty years ago, Theorell and Chance laid the groundwork by proposing a mandatory sequence for binding, starting with the coenzyme and followed by the substrate [13]. Their proposed bi-bi ordered mechanism, that is visually depicted in red

* Corresponding authors at: Department of Physical and Chemical Sciences, University of L'Aquila, via Vetoio (Coppito 1), L'Aquila 67100, Italy (M. Capone).
E-mail addresses: matteo.capone@nano.cnr.it (M. Capone), nicoletta.spreti@univaq.it (N. Spreti).

https://doi.org/10.1016/j.bioorg.2024.107932
Received 7 August 2024; Received in revised form 16 October 2024; Accepted 27 October 2024
Available online 30 October 2024

in Fig. 1, where the cofactor (NADH/NAD$^+$) is the first to bind to the enzyme and the last to leave the active site.

Among various reported reaction steps, the dissociation of the binary E-cofactor product complex was identified as the rate-determining step, as pointed out by Dalziel in 1963 [14]. The kinetic constants of this process were estimated by Plapp through kinetic simulations of a family of progress curves using KIN SIM and FITSIM [15]. This approach allowed establishing the relationships between the kinetic constants and the affinity constant, determining which of the constants was the catalytic one. Specifically, the Michaelis constant serves as a crucial indicator, representing the equilibrium constant governing both the formation and dissociation processes of E-cofactor complexes or E-cofactor-substrate complexes. On the other hand, the catalytic constant delineates the dissociation constant specifically pertaining to the E-cofactor product complex. The described relationships are reported in Table 1.

Meticulous investigations involving initial velocity studies by varying substrate concentrations provided support for the Theorell–Chance mechanism, but more intricate mechanisms emerged from steady-state kinetic studies. Indeed, at least another reaction pattern, that can occur with high relative substrate concentrations, has been proposed [16] (blue path in Fig. 1). According to this reaction mechanism, the enzyme can initially bind the substrate, forming an E-substrate complex to which the cofactor will subsequently bind at different rates depending on the substrate under examination. This process thus influences kinetic parameters. Moreover, the possibility of abortive ternary complexes (*i.e.* non-productive), both in reduction (E-NADH-RCH$_2$OH) and in oxidation (E-NAD$^+$-RCHO) have been proposed. Being the possible number of ternary complexes large and debated, such complexes are not reported in scheme in Fig. 1.

The formation of abortive E–NAD$^+$–aldehyde and E–NADH–alcohol complexes is particularly evident under very high substrate concentrations [17,18]. Notably, when ethanol is the alcohol substrate, NADH dissociates slower from the abortive enzyme–NADH–alcohol complex, showing substrate inhibition. Conversely, with cyclohexanol as the substrate, NADH dissociation occurs more rapidly, demonstrating also substrate activation [19,20]. Additionally, benzyl alcohol forms an abortive enzyme–NADH–alcohol complex, impeding the dissociation of NADH [21]. Product inhibition investigations proved the kinetic importance of the abortive ternary E–cofactor–substrate complexes in the overall reaction scheme. These findings underline the diverse and nuanced effects of different alcohols on the enzyme's behavior, highlighting the complexity of the reaction mechanisms beyond the first proposal [16].

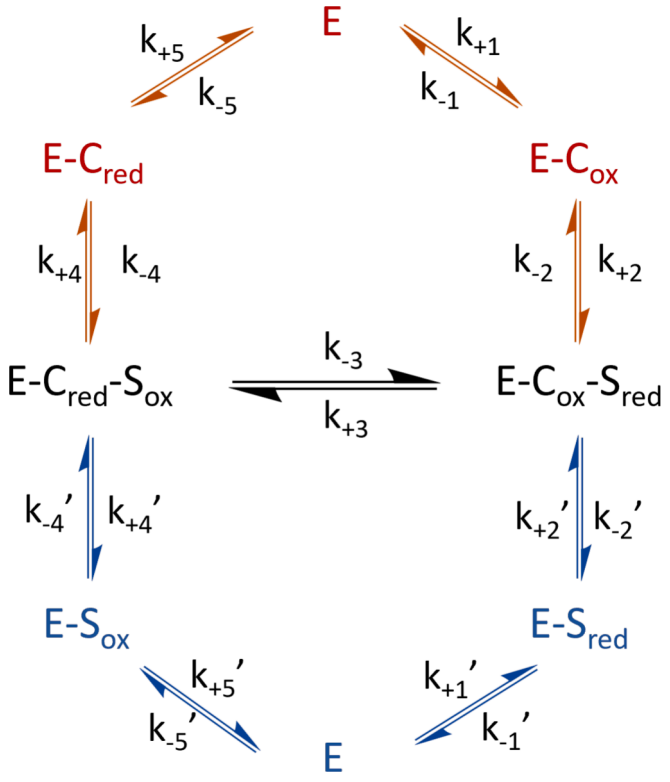

Fig. 1. Global reaction scheme, where C_{red} and C_{ox} are respectively the two forms of the cofactor: NADH and NAD$^+$, and S_{ox} and S_{red} correspond to the carbonyl and alcoholic substrates respectively.

Table 1
Relationship between kinetic constants with both affinity and catalytic constants. All the equations reefer to the main reaction path reported in red in Fig. 1.

oxidation	reduction
$K_M(NAD^+) = \frac{k_{+5}}{k_{+1}}$	$K_M(NADH) = \frac{k_{-1}}{k_{-5}}$
$K_M(RCH_2OH) = \frac{k_{+4}}{k_{+2}}$	$K_M(RCHO) = \frac{k_{-2}}{k_{-4}}$
$k_{cat}(ox) = k_{+5}$	$k_{cat}(red) = k_{-1}$

As just described, HLADH is an extensively studied and well-characterized enzyme from both a kinetic and structural perspective. Specifically, researchers have investigated the impact of substrate structure, inhibition or activation by substrate and product through the formation of ternary complexes, and how enzyme kinetics vary with different metals [16,20,22]. Throughout these explorations, and in practical applications, the cofactor concentration is typically kept constant, at or below than 0.2 mM for the reduction [23,24] and approximately at 1 mM for the oxidation reaction [25,26]. In this study we aimed to investigate the effect of both substrate and cofactor concentration on enzyme activity. In the present work, kinetic anomalies under variable cofactor concentration have been observed. Thus, we used molecular dynamics (MD) simulations to rationalize this behavior at molecular level.

2. Results and discussion

2.1. Measurements of enzyme kinetics

As can be seen from the profile in Fig. 2A, the rate of oxidation reaction for all three substrates increases by increasing cofactor concentration until reaching a plateau at saturating concentration. Instead, as depicted in the profile on the right (Fig. 2B), an unusual pattern was noticed. Contrary to the expected Michaelis–Menten behavior, under varying NADH concentrations, the observed kinetics deviates from the typical model. Rather than reaching a plateau at saturating coenzyme concentrations, the reaction rate initially rises to a maximum, after that it declines. This effect has been previously observed in the case of alcohol dehydrogenase from *Saccharomyces cerevisiae* for the reduction reaction of formaldehyde [27]. In that study, they observed that when the NADH concentration ranged between 8 to 14 mM, the reaction followed Michaelis–Menten kinetics. However, at higher (25–40 mM) or lower (6–8 mM) concentrations of NADH, the enzyme exhibited unconventional behavior, strongly suggesting the presence of a cofactor inhibition phenomenon, although they did not delve into further mechanistic details. In the present work we observed similar inhibition behavior for the reduction reaction in all the three studied substrates. Our results showed more substantial inhibition than has been reported for other enzymes, such as phosphofructokinase-2 (Pfk-2) from *Escherichia coli*, where enzyme inhibition was observed in the presence of high concentrations of ATP [28]. Therefore, this divergence from the conventional Michaelis–Menten kinetics requires a deeper exploration of the underlying factors that influence the reaction behavior with varying

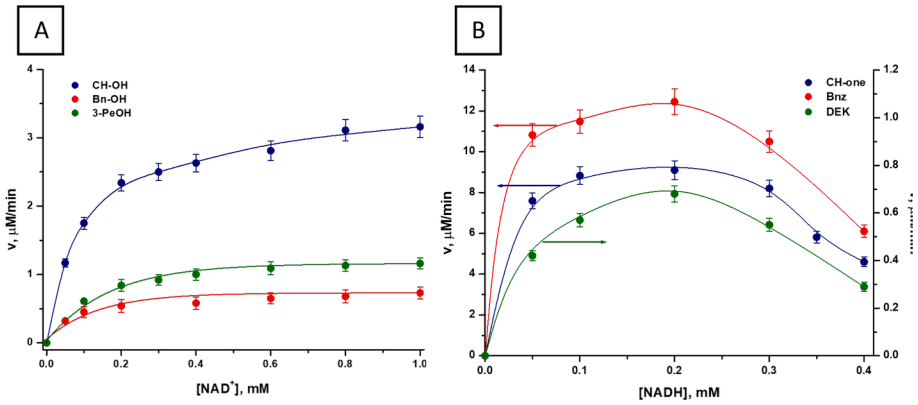

Fig. 2. (A) Effect of NAD^+ concentration on the reaction rate for the three substrates: cyclohexanol (CH-OH), benzyl alcohol (Bn-OH), and 3-pentanol (3-PeOH) on the left; (B) effect of NADH concentration on the reduction reaction rate for the three substrates: cyclohexanone (CH-one), benzaldehyde (Bnz), and 3-pentanone (DEK) on the right.

cofactor concentrations.

Typically, initial rate equations are formulated on the basis of the Michaelis constant. However, as just described, in the case of two-substrate reactions, the Michaelis constant for each substrate (K_M^S) and cofactor (K_M^C) tends to vary with the concentration of the other [19]. The kinetic parameters of both reactions, oxidation and reduction, at non inhibitory cofactor concentrations (0.01–0.05 mM NADH; 0.1–1.0 mM NAD^+), are reported in Table 2.

Enzyme affinity values observed for both alcoholic and carbonyl substrates closely align with those documented in literature [18,21,29–31,10,4]. The high enzyme affinity for benzyl substrates can be reasonably ascribed, at least in part, to the hydrophobic characteristics of its active site. Furthermore, within the entry cavity of the substrate close to the catalytic zinc ion, two specific residues, namely Phe-93 and Phe-319, can establish pi-stacking interactions with the benzyl substrates, contributing to their enhanced affinity for the enzyme. If we consider the mechanism reported in red in Fig. 1 as the sole mechanism, the K_M^C and the reaction k_{cat}, related to steps involving only the enzyme and coenzyme, should not be affected by the substrate. In more detail, the K_M^C represents the equilibrium constant of the cofactor dissociation (consumed)/association (new) process, and the catalytic constant has been identified as the kinetic constant for the cofactor dissociation step, which is the rate determining step [15]. Furthermore, the kinetic parameters can be strongly influenced by the formation of the abortive ternary complexes described above. For example, in the presence of an excess of cyclohexanol, which has a k_{cat} value three times higher than the other two substrates, it has been demonstrated that NADH dissociates more rapidly from the formed abortive ternary complex compared to both ethanol and the product complex E-NADH [19].

In addition to the variable affinity of the cofactor depending on the substrate, it is evident from the reduction reaction data that NADH consistently exhibits in all cases a much greater affinity than its oxidized form. It is precisely in this higher affinity of NADH that we sought the reason for the anomalous behavior observed in the kinetic profile (Fig. 2B). To better understand this behavior, we chose a synergistic computational-kinetic approach. Since the anomalous kinetic trend with increasing NADH concentration appears to be independent of the substrate under examination, cyclohexanone was chosen as substrate for further experiments. This choice was motivated by its convenience from a kinetic perspective. Although it has a high K_M^S, it exhibits a good k_{cat}, and the balance between the two parameters results in a suitable reaction velocity for the experimental set-up. This does not hold true for the reduction reaction of benzaldehyde, which is very fast. Conversely the reaction for pentanone is rather slow due to its very low k_{cat}.

So, to better understand the anomalous behavior from a kinetic point of view, we conducted kinetic analyses of cyclohexanone at different NADH concentrations, ranging from non-inhibitory to inhibitory levels, from 0.05 to 0.5 mM. All lines at different cofactor concentrations are depicted together in a Lineweaver–Burk plot in Figure S1†. The effect of NADH concentration on K_M^S (A) and k_{cat} (B) of cyclohexanone is reported in Fig. 3. From the trend shown in Fig. 3A it is evident that, as the coenzyme concentration increases, there is a noticeable rise in K_M^S, from 6 to 30, going from 0.05 mM to 0.5 mM of NADH, indicating a rapid decrease in the affinity of the enzyme for the substrate. At the same time, the catalytic constant (Fig. 3B) shows a bell-shaped trend, suggesting that the enzyme catalytic efficiency initially increases from 0.4 to 0.8 s^{-1} at 0.3 mM of NADH and then decreases to 0.4 s^{-1} with rising NADH concentration up to 0.5 mM. Based on these experimental results, a simple analysis of K_M^S and k_{cat} values does not provide information on the microscopic mechanisms occurring at inhibitory cofactor concentrations. Therefore, in the following sections, the results obtained from a series of molecular dynamics simulations performed by adding supplementary non-catalytic NADH molecules to clarify this anomalous behavior are reported.

Table 2
The kinetic parameters for the oxidation and reduction reactions by varying both the substrate and cofactor concentrations.

Oxidation			Reduction		
	K_M, mM	k_{cat}, s^{-1}		K_M, mM	k_{cat}, s^{-1}
CH-OH	1.04	0.06	CH-one	7.6	0.3
NAD^+	0.08		NADH	0.03	
Bn-OH	0.03	0.02	Bnz	0.04	0.3
NAD^+	0.09		NADH	0.008	
3-PeOH	3.5	0.02	DEK	0.3	0.003
NAD^+	0.2		NADH	0.004	

2.2. Molecular dynamics simulations

To rationalize the different behavior of HLADH at low and high concentrations of NADH, two sets of molecular dynamics (MD) simulations were conducted. In the first set, labelled as '2-NADH', simulations were performed on the holo-protein with one catalytic NADH and one substrate molecule present in each of the two catalytic sites (see panel A of Fig. 4 for a representative configuration of the active site). According to the X-ray-derived structure [20], the reaction cavity has two potential entrances: a larger one primarily for cofactor binding and a smaller one for substrate binding (see panel A of Fig. 4). In the second set, the simulations were conducted with additional NADH molecules placed in contact with different parts of the enzyme using a docking procedure with the program Vina [32]. Two of the three lowest-energy docking poses have the additional NADH molecule in close proximity to

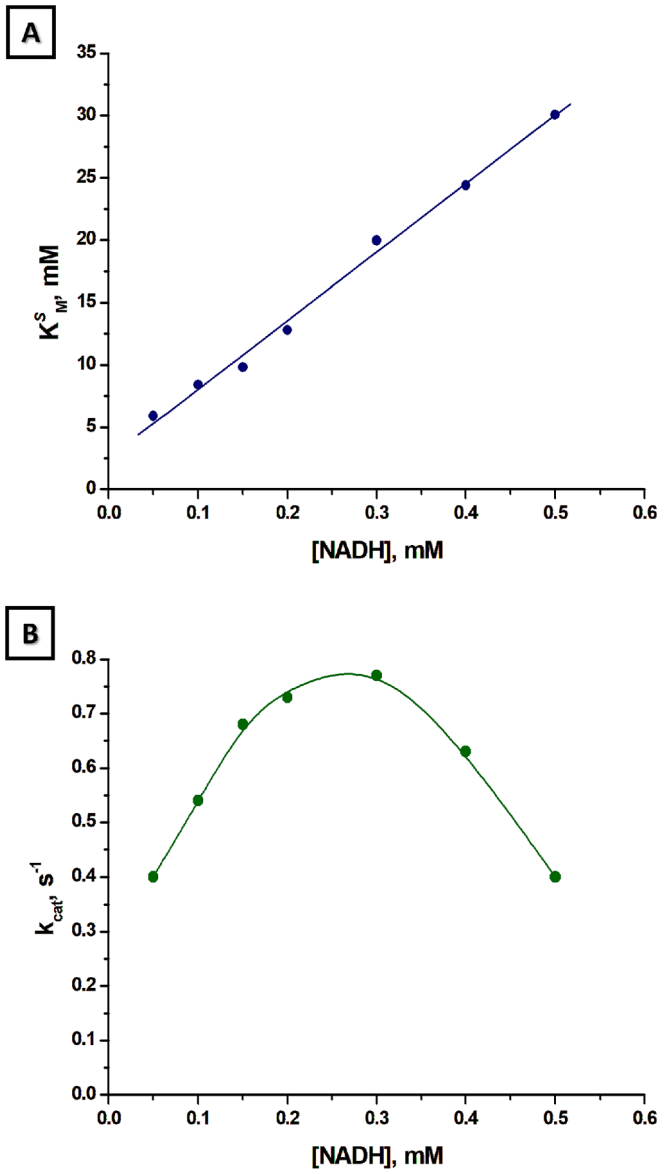

Fig. 3. Trends of K_M^S (A) and k_{cat} (B) of the reduction reaction as coenzyme concentration rises from non-inhibitory to inhibitory range.

the active site, one at the cofactor entrance and the other at the substrate entrance (see Figure S2†). Interestingly, in the lowest-energy docking pose found, the additional NADH molecule is localized on the opposite side of the catalytic site, namely in a cavity between the two subunits of HLADH (see panel B of Fig. 4 for a representative configuration). We refer to this cavity as the allosteric site for the reasons given below. In summary, the three identified docking sites are: (i) at the substrate entrance of the reaction cavity (see Figure S2† panel A†); (ii) at the NADH entrance of the reaction cavity (see Figure S2† panel B); (iii) in the allosteric site, between the two enzyme subunits (Fig. 4 panel B).

Three preliminary 100 ns-long MD simulations were performed starting from the three docked configurations to assess their stability. The Root Mean Square Deviation (RMSD) of the additional NADH molecule with respect to the corresponding starting structure, calculated over the three simulations (reported in Figure S3†), shows that only the allosteric-docked configuration is stable. The residues primarily responsible for stabilizing the additional cofactor molecule at the allosteric site are two Lys188 residues, one in each monomer, which interact with the two phosphate groups of NADH (see Fig. 4 panel B). Additionally, the Glu107 side chains from each monomer play a role in stabilizing the hydroxide from the ribose groups. In the other two cases, the additional NADH molecule instead moves away from its initial position. On the basis of these results, in the following we only consider simulations of the allosteric-docked configurations for comparison with the simulation of the '2-NADH' system. We will refer to this set of simulations as '3-NADH'.

For both the 2-NADH system and the 3-NADH one, we performed three 200 ns parallel simulations using different initial velocities. The Root Mean Square Fluctuation (RMSF) per residue and all the following analysis were then calculated over a total of 600 ns for the 2-NADH system and 510 ns for 3-NADH system (See methods section for additional details). As shown in panel B of Fig. 5, the RMSF is consistently lower in the allosteric-docked system (red line) compared to the 2-NADH system (blue line). This difference is further highlighted by examining the difference of the RMSF per residue between the two systems (black line in the same figure). The figure also highlights the protein regions corresponding to the entrance of the catalytic NADH and the substrate, depicted in Fig. 5A as orange and green regions, respectively. Also, the residues belonging to the allosteric site are shown in blue. The residue indexes corresponding to these regions are similarly highlighted with their respective color palette in the RMSF plot in panel B. Additionally, regions with high structural flexibility are highlighted in pink in both panels. Overall, it is evident that the occupation of the allosteric site induces a global stiffening of the protein structure, as also observed in other enzymes [33], and specifically of the regions corresponding to the access points to the catalytic cavity. For this reason, we named this occupation site as the allosteric site. Residues 50–60 and 295–300, which define the protein surface separating the two entrances (the two green regions in contact, and surrounded by the pink ones), exhibit considerable structural flexibility in the 2-NADH system. In particular, the protein region composed of the residues between Asp50 and Pro60 shows the largest RMSF difference. High fluctuations between these regions result in a widening of the catalytic cavity, forming a unique crevice that exposes both the nicotinamide moiety of the catalytic NADH and the substrate to the solvent. The second region that exhibits the most significant difference between the two sets is formed by residues ranging from Trp15 to Pro20 (pink region). This region has direct interactions with the portions between residues 50 and 60 from each subunit (green regions), thus exhibiting concerted movements with such regions.

To gain a deeper understanding of possible correlated motions induced by the presence of the additional NADH, an essential dynamics (ED) analysis [34–36] was performed using the whole conformational space sampled along all sets of simulations. The ED analysis performed on the backbone atoms revealed that the two systems exhibit quite different dynamics. In fact, projection of the 2-NADH and 3-NADH simulations onto the first eigenvector, which accounts for the largest backbone fluctuations, reveals rather distinct distributions (see Fig. 6). The first eigenvector involves correlated motions of the catalytic cavity and the potentially inhibitory allosteric site. In particular, the motion of the two cavities shows an anti-correlated behavior: as the catalytic cavities widen, the allosteric site contracts, and vice versa. Generally, in the 2-NADH simulations, the enzyme shows broader catalytic cavities (blue line in Fig. 6), resulting in a smaller size of the cavity that could accommodate the additional NADH.

Conversely, in the 3-NADH simulations, the presence of the additional NADH leads to a widening of the allosteric site and a narrowing of the catalytic site. This result is consistent with data reported in a crystallographic study [15] in which the catalytic site occupation was shown to induce a tilt of the two subunits, resulting in a "squeezing" of the cavity present between the two monomers. Hence, it is plausible to speculate that such a cavity may serve as a true allosteric site, influencing the geometric features of the catalytic site located on the opposite side of the enzyme.

On the basis of the structural and dynamical features derived from the computational data, it is possible to hypothesize a molecular

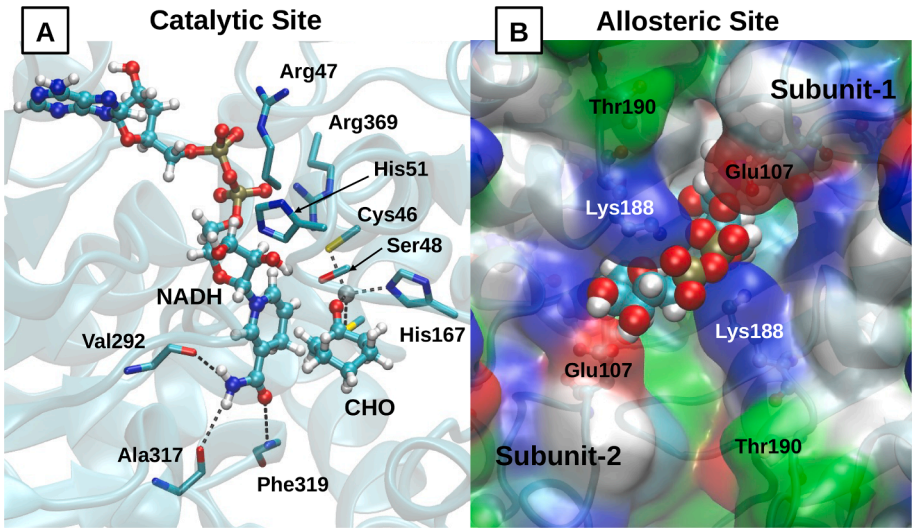

Fig. 4. Representative structure of the NADH cofactor in the catalytic site (A) and allosteric site (B). In panel A the interactions with Arg47, Val292, Ala317, Phe319, and Arg369 that stabilize the NADH in the catalytic site are highlighted. In panel B the interactions with the two Lys188 and Glu107, which constitute the allosteric pocket for the additional NADH, are highlighted.

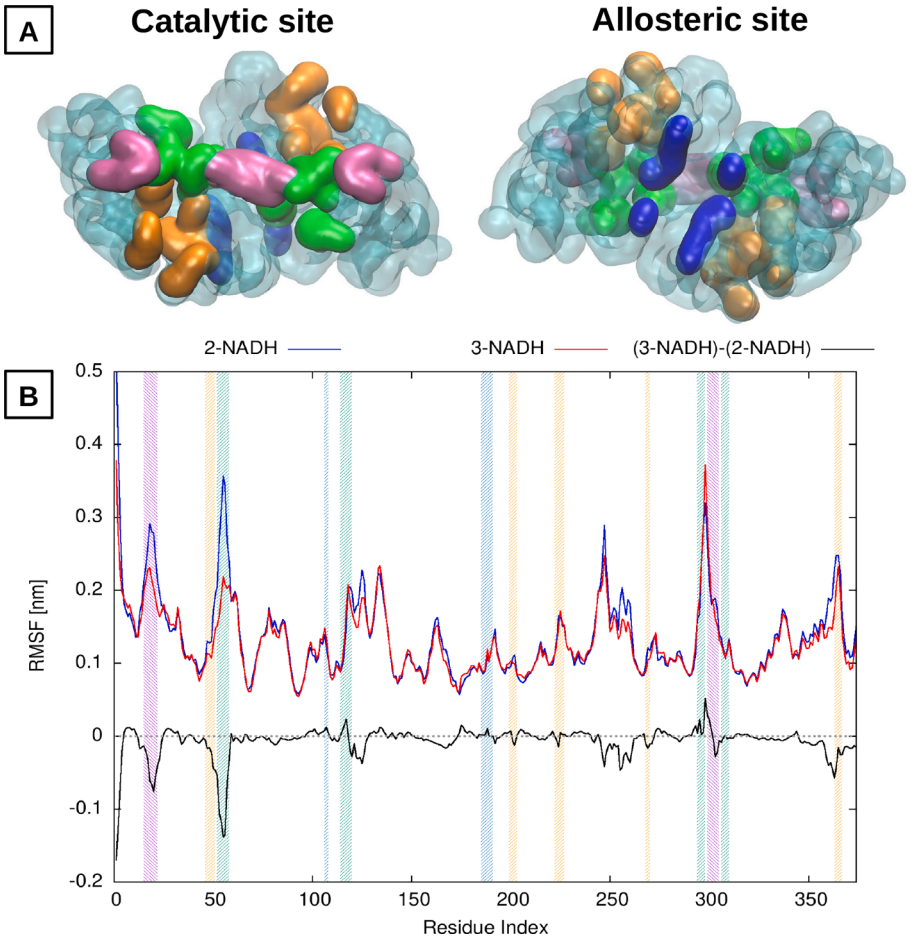

Fig. 5. The protein and its secondary structure elements are reported in transparency in panel A. The protein portion constituting the NADH cavity (orange), the substrate cavity (green) and allosteric cavity (blue) are highlighted. The pink regions correspond to residues that are not directly connected to the catalytic site, but are strongly influenced by the NADH inhibition effect in the simulations. Root Mean Square Fluctuation per residue averaged over the two subunits for the two sets of simulations are shown in panel B. The RMSF difference between the 3-NADH simulations and 2-NADH ones is also reported in black. The residues constituting the substrate and NADH cavity are reported in green and orange, respectively. Also two regions with a significant RMSF variation, but not corresponding to any specific cavity, are reported in pink.

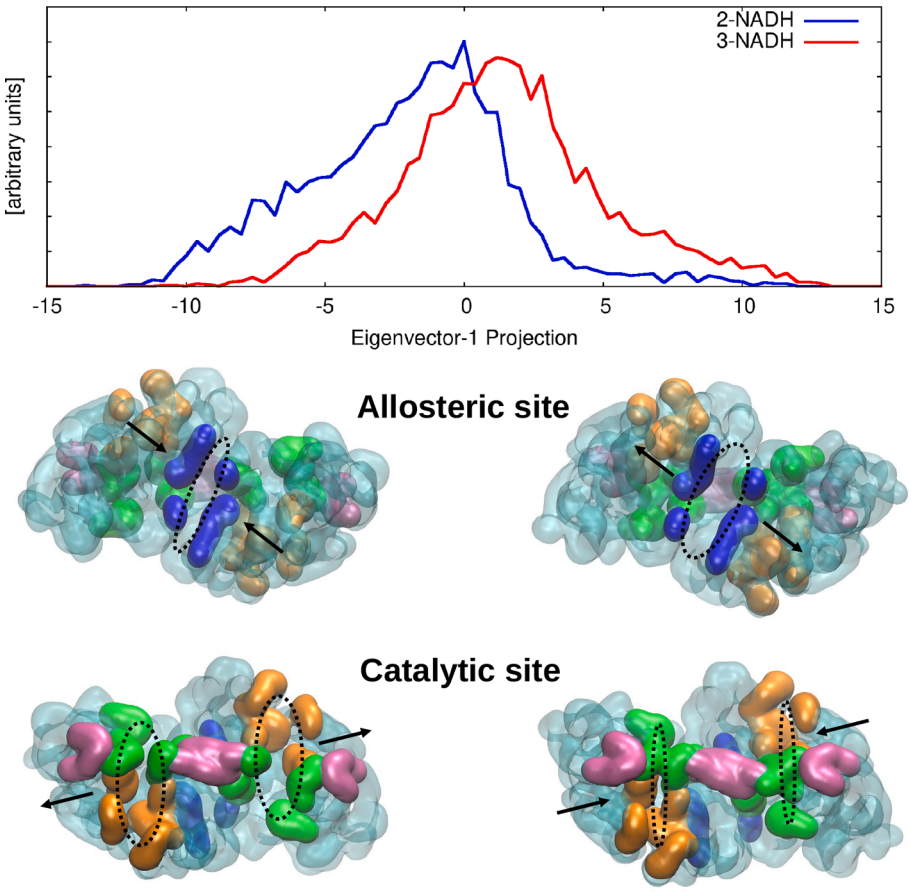

Fig. 6. Projection of the systems' configurations sampled in the 2-NADH and 3-NADH MD simulations on the first eigenvector obtained from an Essential Dynamics analysis of the backbone atoms. Negative values correspond to a wider reaction site and smaller allosteric cavity. Conversely, positive values correspond to a narrower reaction site and a larger allosteric cavity. The protein region corresponding to the entrance of the catalytic NADH is highlighted in orange, the one corresponding to the substrate entrance in green and the allosteric cavity in blue.

rationale behind the unconventional kinetic behavior of HLADH. Concerning the measured k_{cat}, two distinct regimes were observed at low and high concentrations of NADH: up to a 0.2 mM (i.e. at non-inhibitory NADH concentrations), the k_{cat} increases, as expected for a Michaelis–Menten scheme; after reaching this turning point (i.e. at inhibitory NADH concentrations), the k_{cat} decreases.

We attribute this effect to the presence of the NADH cofactor, not only in the catalytic cavity but also in the allosteric site. Previous studies [15] identified the reaction mechanism depicted in red in Fig. 1 as the prevalent path. The alternative scenario depicted in blue, where the substrate/product is associated/released before the cofactor, has been proposed as a minor path. For the first reaction pathway in the scheme, the rate-limiting step (k_{cat}) is associated with the release of the "exhausted" cofactor, NAD^+. Although no rate-limiting step was clearly identified for the second path, it is reasonable to expect that, also in this scenario, the release of the product or the exhausted cofactor remains the rate-limiting step. In both mechanisms, the overall increased stiffness induced by the presence of the allosteric NADH would inevitably reduce the ability of the protein to release either the cofactor or the product after the conversion. Therefore, the critical concentration value can be associated with the point in which a significant amount of the enzymes in solution have an occupied allosteric site.

Understanding the molecular determinants associated with the regulation of non-conventional binding sites, including allosteric and cryptic sites, can play a critical role in pharmaceutical compound design and, consequently, in medical treatments [37,38]. Unlike traditional active sites, these non-canonical or hidden sites offer novel strategies for therapeutic intervention, as they can modulate protein function in ways that are often more specific and less prone to resistance development. In this context, several approaches have been employed, ranging from scoring function-based binding programs [32] and water interface sampling [39], to neural networks [40]. However, MD-based refinement has been shown to significantly improve results derived from static structures. MD simulation not only helps identify the key molecular determinants that characterize these interactions but also reveals the conformational dynamics within the binding site [41,42]. The behavior of HLADH, in particular, suggests possible dynamic responses to environmental or cellular signals, which might serve a biological function, such as a negative feedback mechanism triggered by excess NADH, preventing the over-reduction of critical biomolecules. Below, we propose also a speculative explanation for the observed linear increase in K_M^S with increasing NADH concentration. This type of behaviour has been observed also by others [19,27] but it was not discussed in detail. An increase of K_M^S could be explained by a decrease in the association rate of the substrate (which is at the denominator of K_M^S), and/or an increase in the dissociation rate of the product (which is at the numerator of K_M^S). The formation of the active E-cofactor-substrate ternary complex can be obtained either by an early association of the substrate to the apo-enzyme (k_{-5}' in the blue path of Fig. 1) or by its binding to the E-NADH complex (k_{-4} in the red path of Fig. 1). If both pathways are active, as proved in previous studies [16], the apparent substrate association constant will be a combination of the two. Therefore, the variation in the relative population of the two paths will affect the K_M^S value. As reported in a previous crystallographic studies [15,43], the association of the cofactor in the primary mechanism induces a conformational

change that reduces size of the reaction cavity. Thus, we can assume that k_{-4} is smaller than k_{-5}'. Given that the amount of E-NADH complex depends on the NADH concentration, the increase in the latter will further shift the reaction ratio in favor of the early association of the cofactor, resulting in a slower substrate association constant. This effect can explain the NADH-dependent decrease of the denominator of K_M^S, resulting in an increase of K_M^S.

Although after the catalytic reaction step no other step is directly influenced by the NADH concentration, a possible increase of the product dissociation rate in the primary mechanism (red path in Fig. 1) can be explained by the formation of an abortive ternary complex E-ROH-NADH. This ternary complex would result from replacing the oxidized NAD^+ with a new NADH after the catalytic reduction reaction but before the release of the ROH product. From this branch, it has been proposed that both the product and the NADH would dissociate more rapidly than the product alone due to the interaction with a non-affine counterpart [19]. The formation of this complex would depend on the NADH concentration and, as its concentration increases, the likelihood of E-NADH-ROH complex formation would also increase. If the product dissociates more rapidly from this abortive ternary complex, this implies an increase in the apparent dissociation constant. This results in an increase in the numerator of K_M^S, and consequently, of K_M^S itself. Although the hypothesis of the discussed abortive ternary complex is not directly supported by measurements, it can help to explain the increase in K_M^S with the increasing cofactor concentration.

3. Conclusions

The study presented here on Horse Liver Alcohol Dehydrogenase (HLADH) offers a profound understanding of its kinetic behavior and structural dynamics, unraveling complex mechanisms governing its catalytic activity and cofactor interactions. Deviation from traditional Michaelis–Menten kinetics, showcasing a slowdown in the catalytic rate in the presence of high NADH concentrations, is observed. Through molecular dynamics simulations, a potential allosteric site is identified, elucidating how excessive cofactor concentrations influence protein dynamics and catalytic properties. Specifically, structural changes induced by inhibitory NADH concentrations are demonstrated to reduce protein flexibility and alter the size of the catalytic cavities, offering insights into the inhibitory mechanism at high cofactor concentrations. This comprehensive investigation into HLADH's kinetics and structural dynamics has revealed intricate aspects of its catalytic mechanisms, laying a foundation for further exploration in enzymology.

4. Materials and methods

4.1. Materials

Horse Liver Alcohol Dehydrogenase (HLADH recombinant, expressed in E. coli, ⩾0.5 U/mg), β-nicotinamide adenine dinucleotide hydrate (NAD^+, grade ⩾96.5%), nicotinamide adenine dinucleotide reduced (NADH, grade ⩾94.0%), cyclohexanol (CH-OH), cyclohexanone (CH-ONE), 3-pentanone (DEK), 3-pentanol (3-PeOH), benzaldehyde (Bnz) and benzyl alcohol (Bn-OH) were purchased from Merck. Enzyme and substrate were used with no further purification. All other chemicals used were of analytical grade.

4.1.1. Kinetic profiles

The catalytic activity of HLADH was evaluated through the oxidation of cyclohexanol, 3-pentanol and benzyl alcohol into products, coupled with the simultaneous reduction reaction of NAD^+ into NADH, and vice versa. The standard assay was performed at 25.0 °C in a Tris–HCl buffer solution (50 mM, pH 8.0) containing a substrate concentration of 10 mM. The cofactor concentrations were varied to establish the enzyme's kinetic profile, specifically NAD^+ ranging from 0 to 1.0 mM and NADH from 0 to 0.4 mM. The enzyme concentration was maintained at 0.5 μM, except for DEK, where it was set at 1 μM. Enzyme activity measurements were conducted through spectrophotometric kinetics at a wavelength of 340 nm, monitoring the changes in NADH absorbance. These measurements were performed using a Shimadzu UV-160A instrument, and each assay was repeated three times for accuracy and reliability.

4.1.2. Kinetic parameters

A set of initial rate measurements was conducted. Initially, the substrate concentration was kept constant while varying that of the cofactor (0.01–0.5 mM NADH; 0.1–1.0 mM NAD^+). Subsequently, this process was reversed, maintaining the cofactor concentration constant while altering that of the substrate (1.0–10.0 mM). These systematic measurements were aimed at elucidating and determining the affinity and catalytic constants associated with both the substrate and the cofactor in the enzymatic reaction.

4.2. Computational methods

Two sets of molecular dynamics simulations were performed. One set was carried out on the holo-protein, named '2-NADH', which included one substrate molecule (cyclohexanone) and one cofactor molecule (NADH) in each monomer of the enzyme. The other set aimed to replicate a higher NADH concentration. To achieve this goal, molecular docking techniques were utilized to identify optimal poses for additional NADH molecules. Using the autodock-tools [44] and Vina [32] programs, three possible docked conformations for an inhibiting NADH molecule were identified: (i) one at the entrance of the substrate cavity (Figure S2† panel A); (ii) one at the entrance of the NADH cavity (Figure S2† panel B); (iii) one between the two enzyme subunits (Fig. 4). As docking parameters, a cubic box of 40 Å side centered at the cavity entrances and an exhaustiveness of 40 have been used. The center of each box has been placed at the center of each studied cavity. The binding energy provide for the three selected docked conformations are −7.4 kcal/mol for dockings (i) and (ii), whereas is slightly more negative for the docking (iii) with −7.7 kcal/mol. For the MD simulations starting from docking (i) and (ii), the additional NADH molecule was placed in both monomers. A 100 ns-long MD simulation was performed for each docked configuration. Given that in the MD simulations started from docking (i) and (ii) the additional NADH molecules did not remain stably interacting with the enzyme (see the RMSD in Figure S3†), only the (iii)-docked system is discussed in the Results section. This system was named '3-NADH'.

To enhance the conformational sampling of the 2-NADH system, the simulation time was extended to 200 ns-long MD and replicated 2 other times with different initial velocities. The protein is observed to be stable as shown by the RMSD of the backbone reported in Figure S4†. For the 3-NADH system, three MD replicas has been carried on as well, however the additional NADH did not remained in the cavity for the entirety of the simulations in all the cases. In the first replica the NADH has left the pocked after 110 ns (See Figure S5†). In the two other replicas, the NADH remained stable for the entire 200 ns of simulation. Thus, the structural analyses discussed in the results have been done on 600 ns for the 2-NADH system and 510 ns for the 3-NADH system as well.

All MD simulations were executed using the GROMACS program [45]. The V-rescale algorithm for temperature coupling at 298 K[46] and the Berendsen algorithm for pressure coupling at 1 atm [47] were employed. The LINCS algorithm was used to constrain the bond lengths involving an hydrogen atom[48]. Short-range interactions were calculated within a cutoff radius of 0.9 nm, while long-range interactions were treated using the PME method [49]. The initial structure of horse liver alcohol dehydrogenase was obtained from the Protein Data Bank, specifically using the pdb 7K35 entry [20]. The units of (4-methylphenyl) methanol (VTG) and (4R)-2-methylpentane-2,4-diol (MRD) present in the file were removed and substituted with cyclohexanone (CHO) with the same orientation. The structural water of hydration

present in the PBD were retained. For the protein, substrate and cofactor the AMBER99 [50] force field was employed. The structures of NADH and substrate (CHO) were optimized using GAUSSIAN16 [51] with the B3LYP functional [52] and the 6-31G basis set and their topology was obtained with the ACPYPE tool [53] that employs GAFF [54] parameters. The tetrahedral catalytic Zn ion coordination was treated using a bonded scheme with the bond and angle parameters taken from Ref [55].

Declaration of Competing Interest

The authors declare that they have no known competing financial interests or personal relationships that could have appeared to influence the work reported in this paper.

Data availability

Data will be made available on request.

Acknowledgements

We acknowledge the use of ChatGPT (https://chat.openai.com/) to identify improvements in the writing style. We thank the Italian supercomputing center CINECA for the computational resources. Prof. I.D. acknowledges financial support by European Union - NextGenerationEU under the Italian Ministry of University and Research (MUR) National Innovation Ecosystem grant ECS00000041 - VITALITY - CUP E13C22001060006.

Appendix A. Supplementary material

Supplementary data associated with this article can be found, in the online version, at https://doi.org/10.1016/j.bioorg.2024.107932.

References

[1] M.A. Maria-Solano, A. Romero-Rivera, S. Osuna, Exploring the reversal of enantioselectivity on a zinc-dependent alcohol dehydrogenase, Org. Biomol. Chem. 15 (19) (2017) 4122–4129.
[2] G. Schneider, H. Eklund, E. Cedergren-Zeppezauer, M. Zeppezauer, Structure of the complex of active site metal-depleted horse liver alcohol dehydrogenase and nadh, EMBO J. 2 (5) (1983) 685–689.
[3] N. Zhang, J.P. Bittner, M. Fiedler, T. Beretta, P.D. De María, S. Jakobtorweihen, S. Kara, Unraveling alcohol dehydrogenase catalysis in organic–aqueous biphasic systems combining experiments and molecular dynamics simulations, ACS Catal. 12 (15) (2022) 9171–9180.
[4] D. Giacomini, P. Galletti, A. Quintavalla, G. Gucciardo, F. Paradisi, Highly efficient asymmetric reduction of arylpropionic aldehydes by horse liver alcohol dehydrogenase through dynamic kinetic resolution, Chem. Comm. 39 (2007) 4038–4040.
[5] O. De Smidt, J.C. Du Preez, J. Albertyn, The alcohol dehydrogenases of saccharomyces cerevisiae: a comprehensive review, FEMS Yeast Res. 8 (7) (2008) 967–978.
[6] A.A. Koesoema, D.M. Standley, T. Senda, T. Matsuda, Impact and relevance of alcohol dehydrogenase enantioselectivities on biotechnological applications, Applied microbiology and biotechnology 104 (7) (2020) 2897–2909.
[7] M.M. Musa, R.S. Phillips, Recent advances in alcohol dehydrogenase-catalyzed asymmetric production of hydrophobic alcohols, Catalysis Science & Technology 1 (8) (2011) 1311–1323.
[8] H. Jørnvall, Horse liver alcohol dehydrogenase: The primary structure of the protein chain of the ethanol-active isoenzyme, Eur. J. Biochem. 16 (1) (1970) 25–40.
[9] H. Eklund, B. Plapp, J. Samama, C. Brändén, Binding of substrate in a ternary complex of horse liver alcohol dehydrogenase, J. Bio. Chem. 257 (23) (1982) 14349–14358.
[10] J. Jeffery, J. Chesters, C. Mills, P. Sadler, H. Jörnvall, Sorbitol dehydrogenase is a zinc enzyme, The EMBO Journal 3 (2) (1984) 357–360.
[11] H. Jörnvall, H. von Bahr-Lindström, J. Jeffrey, Extensive variations and basic features in the alcohol dehydrogenase–sorbitol dehydrogenase family, Eur. J. Biochem. 140 (1) (1984) 17–23.
[12] J. Jeloková, C. Karlsson, M. Estonius, H. Jörnvall, J.-O. Höög, Features of structural zinc in mammalian alcohol dehydrogenase: Site-directed mutagenesis of the zinc ligands, Eur. J. Biochem. 225 (3) (1994) 1015–1019.
[13] K. Dalziel, Kinetic studies of liver alcohol dehydrogenase, Biochem. J. 84 (2) (1962) 244.
[14] K. Dalziel, Thermodynamics and molecular kinetics of liver alcohol dehydrogenase, Acta Chem Scand 17 (1963) 27–33.
[15] B.V. Plapp, Conformational changes and catalysis by alcohol dehydrogenase, Arch. Biochem. Biophys. 493 (1) (2010) 3–12.
[16] K. Dalziel, F. Dickinson, The kinetics and mechanism of liver alcohol dehydrogenase with primary and secondary alcohols as substrates, Biochem J. 100 (1966) 34–46.
[17] F. Dickinson, K. Dalziel, The specificities and configurations of ternary complexes of yeast and liver alcohol dehydrogenases, Biochem J. 104 (1967) 165–172.
[18] V. Sekhar, B. Plapp, Rate constants for a mechanism including intermediates in the interconversion of ternary complexes by horse liver alcohol dehydrogenase, Biochemistry 29 (1990) 4289–4295.
[19] K. Dalziel, F. Dickinson, Substrate activation and inhibition in coenzyme-substrate reactions cyclohexanol oxidation catalysed by liver alcohol dehydrogenase, Biochem J. 100 (1966) 491–500.
[20] B.V. Plapp, R. Subramanian, Alternative binding modes in abortive nadh-alcohol complexes of horse liver alcohol dehydrogenase, Arch. Biochem. Biophys. 701 (2021) 108825.
[21] G. Shearer, K. Kim, K. Lee, C. Wang, B. Plapp, Alternative pathways and reactions of benzyl alcohol and benzaldehyde with horse liver alcohol dehydrogenase, Biochemistry 1 (1993) 11186–11194.
[22] D. Sigman, Interactions of substrates, inhibitors, and coenzymes at the active site of horse liver alcohol dehydrogenase, J. Biol. Chem. 242 (1967) 3815–3824.
[23] S. Chanquia, L. Huang, G. Liñares, P. de María, S. Kara, Deep eutectic solvents as smart cosubstrate in alcohol dehydrogenase-catalyzed reductions, Catalysts 10 (2020) 1–8.
[24] T. Itozawa, H. Kise, Hladh-catalyzed reduction of cyclohexanone with nadh regeneration by alcohols: Effects of reaction conditions, Bull. Chem. Soc. Jpn. 67 (1994) 3304–3308.
[25] R. Kemper, A. Elfarra, Oxidation of 3-butene-1,2-diol by alcohol dehydrogenase, Chem. Res. Toxicol. 9 (1996) 1127–1134.
[26] C. Dithugoe, J. van Marwijk, M. Smit, D. Opperman, An alcohol dehydrogenase from the short-chain dehydrogenase/reductase family of enzymes for the lactonization of hexane-1,6-diol, ChemBioChem 20 (2019) 96–102.
[27] N. Wen, W. Liu, Y. Hou, Z. Zhao, The kinetics behavior of the reduction of formaldehyde catalyzed by alcohol dehydrogenase (adh) and partial uncompetitive substrate inhibition by nadh, Appl. Biochem. Biotechnol. 170 (2013) 370–380.
[28] R. Cabrera, M. Baez, H.M. Pereira, A. Caniuguir, R.C. Garratt, J. Babul, The crystal complex of phosphofructokinase-2 of escherichia coli with fructose-6-phosphate: kinetic and structural analysis of the allosteric atp inhibition, J. Biol. Chem. 286 (7) (2011) 5774–5783.
[29] M. Andersson, P. Adlercreutz, Evaluation of simple enzyme kinetics by response surface modelling, Biotechnol. Tech. 13 (1999) 903–907.
[30] A. Irwin, K. Lok, K. Huang, B. Jones, Enzymes in organic synthesis. influence of substrate structure on rates of horse liver alcohol dehydrogenase-catalysed oxidoreductions, J. Chem. Soc., Perkin Trans. 12 (1978) 1636–1642.
[31] R. Pietriszico, K. Crawford, D. Lester, Comparison of substrate specificity of alcohol dehydrogenases from human liver, horse liver, and yeast towards saturated and 2-enoic alcohols and aldehydes, Arch. Biochem. Biophys. 159 (1973) 50–60.
[32] O. Trott, A.J. Olson, Autodock vina: Improving the speed and accuracy of docking with a new scoring function, efficient optimization, and multithreading, J. Comp. Chem. 31 (2) (2010) 455–461, https://doi.org/10.1002/jcc.21334.
[33] M. Zahran, I. Daidone, J.C. Smith, P. Imhof, Mechanism of dna recognition by the restriction enzyme ecorv, J. Mol. Biol. 401 (3) (2010) 415–432.
[34] I. Daidone, D. Roccatano, S. Hayward, Investigating the accessibility of the closed domain conformation of citrate synthase using essential dynamics sampling, J. Mol. Biol. 339 (3) (2004) 515–525.
[35] I. Daidone, A. Amadei, Essential dynamics: foundation and applications, Wiley Interdiscip. Rev. Comput. Mol. Sci. 2 (5) (2012) 762–770.
[36] L. Zanetti-Polzi, S. Corni, I. Daidone, A. Amadei, Extending the essential dynamics analysis to investigate molecular properties: application to the redox potential of proteins, Phys. Chem. Chem. Phys. 18 (27) (2016) 18450–18459.
[37] G. Colombo, Computing allostery: from the understanding of biomolecular regulation and the discovery of cryptic sites to molecular design, Curr. Opin. Struct. Biol. 83 (2023) 102702.
[38] A. Triveri, C. Sanchez-Martin, L. Torielli, S.A. Serapian, F. Marchetti, G. D'Acerno, V. Pirota, M. Castelli, E. Moroni, M. Ferraro, P. Quadrelli, A. Rasola, G. Colombo, Protein allostery and ligand design: Computational design meets experiments to discover novel chemical probes, J. Mol. Biol. 434 (17) (2022) 167468.
[39] F. Comitani, F.L. Gervasio, Exploring cryptic pockets formation in targets of pharmaceutical interest with swish, J. Chem. Theory Comput. 14 (6) (2018) 3321–3331.
[40] A. Meller, M.D. Ward, J.H. Borowsky, J.M. Lotthammer, M. Kshirsagar, F. Oviedo, J.L. Ferres, G. Bowman, Predicting the locations of cryptic pockets from single protein structures using the pocketminer graph neural network, Biophys. J. 122 (3) (2023) 445a.
[41] A.A. Al-Karmalawy, M.A. Dahab, A.M. Metwaly, S.S. Elhady, E.B. Elkaeed, I. H. Eissa, K.M. Darwish, Molecular docking and dynamics simulation revealed the potential inhibitory activity of aceis against sars-cov-2 targeting the h ace2 receptor, Frontiers in Chemistry 9 (2021) 661230.
[42] H. Guterres, W. Im, Improving protein-ligand docking results with high-throughput molecular dynamics simulations, J. Chem. Inf. Model. 60 (4) (2020) 2189–2198.
[43] F. Chen, P. Wang, Y. An, J. Huang, Y. Xu, Structural insight into the conformational change of alcohol dehydrogenase from arabidopsis thaliana l. during coenzyme binding, Biochimie 108 (2015) 33–39.

[44] G.M. Morris, R. Huey, W. Lindstrom, M.F. Sanner, R.K. Belew, D.S. Goodsell, A. J. Olson, Autodock4 and autodocktools4: Automated docking with selective receptor flexibility, J. Comp. Chem. 30 (16) (2009) 2785–2791.
[45] D. Van Der Spoel, E. Lindahl, B. Hess, G. Groenhof, A.E. Mark, H.J. Berendsen, Gromacs: fast, flexible, and free, J. Comp. Chem. 26 (16) (2005) 1701–1718.
[46] G. Bussi, D. Donadio, M. Parrinello, Canonical sampling through velocity rescaling, Chem. Phys. 126 (1) (2007) 014101.
[47] H.J. Berendsen, J.v. Postma, W.F. Van Gunsteren, A. DiNola, J.R. Haak, Molecular dynamics with coupling to an external bath, J. Chem. Phys. 81 (8) (1984) 3684–3690.
[48] B. Hess, H. Bekker, H.J. Berendsen, J.G. Fraaije, Lincs: A linear constraint solver for molecular simulations, J. Comp. Chem. 18 (12) (1997) 1463–1472.
[49] U. Essmann, L. Perera, M.L. Berkowitz, T. Darden, H. Lee, L.G. Pedersen, A smooth particle mesh ewald method, J. Chem. Phys. 103 (19) (1995) 8577–8593.
[50] J.W. Ponder, D.A. Case, Force fields for protein simulations, Adv. Protein Chem. 66 (2003) 27–85.
[51] M.J. Frisch, G.W. Trucks, H.B. Schlegel, G.E. Scuseria, M.A. Robb, J.R. Cheeseman, G. Scalmani, V. Barone, G.A. Petersson, H. Nakatsuji, X. Li, M. Caricato, A. V. Marenich, J. Bloino, B.G. Janesko, R. Gomperts, B. Mennucci, H.P. Hratchian, J. V. Ortiz, A.F. Izmaylov, J.L. Sonnenberg, D. Williams-Young, F. Ding, F. Lipparini, F. Egidi, J. Goings, B. Peng, A. Petrone, T. Henderson, D. Ranasinghe, V. G. Zakrzewski, J. Gao, N. Rega, G. Zheng, W. Liang, M. Hada, M. Ehara, K. Toyota, R. Fukuda, J. Hasegawa, M. Ishida, T. Nakajima, Y. Honda, O. Kitao, H. Nakai, T. Vreven, K. Throssell, J.A. Montgomery Jr., J.E. Peralta, F. Ogliaro, M. J. Bearpark, J.J. Heyd, E.N. Brothers, K.N. Kudin, V.N. Staroverov, T.A. Keith, R. Kobayashi, J. Normand, K. Raghavachari, A.P. Rendell, J.C. Burant, S.S. Iyengar, J. Tomasi, M. Cossi, J.M. Millam, M. Klene, C. Adamo, R. Cammi, J.W. Ochterski, R.L. Martin, K. Morokuma, O. Farkas, J.B. Foresman, D.J. Fox, Gaussian16 Revision C.01, gaussian Inc. Wallingford CT, 2016.
[52] A.D. Becke, Density-functional thermochemistry. i. the effect of the exchange-only gradient correction, J. Chem. Phys. 96 (3) (1992) 2155–2160.
[53] A.W. Sousa da Silva, W.F. Vranken, Acpype-antechamber python parser interface, BMC research notes 5 (2012) 1–8.
[54] W.D. Cornell, P. Cieplak, C.I. Bayly, I.R. Gould, K.M. Merz, D.M. Ferguson, D. C. Spellmeyer, T. Fox, J.W. Caldwell, P.A. Kollman, A second generation force field for the simulation of proteins, nucleic acids, and organic molecules, J. Am. Chem. Soc. 117 (19) (1995) 5179–5197, https://doi.org/10.1021/ja00124a002.
[55] W. Li, J. Zhang, J. Wang, W. Wang, Metal-coupled folding of cys2his2 zinc-finger, J. Am. Chem. Soc. 130 (3) (2008) 892–900.